Eur. Phys. J. B **62**, 59–64 (2008)
DOI: 10.1140/epjb/e2008-00125-x

THE EUROPEAN PHYSICAL JOURNAL B

Magnon scattering by a symmetric atomic well in free standing very thin magnetic films

R. Tigrine[1,2], A. Khater[1,3,a], B. Bourahla[1,2], M. Abou Ghantous[4], and O. Rafil[2]

[1] Laboratoire de Physique de l'État Condensé UMR 6087, Université du Maine, 72085 Le Mans, France
[2] Laboratoire de Physique et Chimie Quantique, Université Mouloud Mammeri, 15000 Tizi-Ouzou, Algérie
[3] Department of Physics, McGill University, 3600 rue University, Montreal, QC H3A 2T8, Canada
[4] Faculty of Natural and Applied Sciences, Notre Dame University, Louaizé, Lebanon

Received 24 March 2007 / Received in final form 18 February 2008
Published online 21 March 2008 –

Abstract. A theoretical model is presented for the study of the scattering of magnons at an extended symmetric atomic well in very thin magnetic films. The thin film consists of three cubic atomic planes with ordered spins coupled by Heisenberg exchange, and the system is supported on a non-magnetic substrate, and considered otherwise free from magnetic interactions. The coherent transmission and reflection scattering coefficients are derived as elements of a Landauer type scattering matrix. Transmission and reflection scattering cross sections are hence calculated specifically, as a function of the varying local magnetic exchange on the inhomogeneous boundary. Detailed numerical results for the individual incident film magnons, and for the calculated overall magnon conductance, show characteristic transmission properties, with associated Fano resonances, depending on the magnetic boundary conditions and on the magnon incidence.

PACS. 75.30.Ds Spin waves – 75.70.Ak Magnetic properties of monolayers and thin films – 75.75.+a Magnetic properties of nanostructures

1 Introduction

Using modern techniques it is possible to prepare well-defined nanostructures as constitutive elements of mesoscopic systems in a variety of devices. The study of nanostructures in general, and *at surfaces* in particular, has been the subject of major research efforts in recent years. There is, as a consequence, an increasing volume of experimental data to elucidate the structural [1–4], magnetic [5–7], and electronic [8–11], properties of finite quasi-1D nanostructures on surfaces.

Scattering and localisation phenomena in low dimensional systems have also been of interest. They are now of renewed interest in the context of modern devices. Most of the recent research in this area has been oriented towards the study of electronic scattering in quasi-one-dimensional systems. The understanding of coherent electronic transport in the mesoscopic regime and its generalization to multi-terminal systems have been provided by the formalism of Landauer [12], and Büttiker [13], who related the conductance of the system to its scattering matrix.

Multiple scattering and quantum interference are not limited, however, to the sole area of electronic transport. In a variety of problems they can become important for the coherent transport of other types of excitations via nanostructures embedded in low dimensional systems [14–17].

Because of the relevance of spin dynamics in certain devices for information processing, the problem of localized magnons, in particular [18], and of their coherent transport has received some attention recently. At low temperatures, these devices are mesoscopic in the sense that their quantum states must be described by coherent wave functions extending over the entire system, and quantum-mechanical interference effects become important [19]. This is illustrated recently for spin currents in mesoscopic Heisenberg systems [20].

The subject of magnon scattering at a surface imperfection in ultrathin films has been considered in the past [21]. In previous work we have also systematically studied the spin dynamics across an inhomogeneous atomic boundary separating ultrathin Heisenberg ferromagnetic films [22], and the magnon coherent conductance via atomic nanocontacts [23]. Our general purpose is to contribute to the understanding of coherent magnon scattering and transmission in magnetic circuits and via nanojuntions. Theses problem are fundamental for applications in magnon devices operating in the coherent regime.

It has been shown [22,23], that the conductance characteristics of Fano resonances play a preferential and important role for the magnon conductance. This effect [24],

[a] e-mail: antoine.khater@univ-lemans.fr

is known in various branches of condensed matter physics. Since the Fano conductance characteristics are modified in different situations and for different nanogeometries, we present in this work a model for the study of coherent magnon transport via an extended atomic well which constitutes the inhomogeneous boundary between two very thin magnetic films. The system is supported on a non-magnetic substrate, and considered otherwise free from magnetic interactions. Present nanotechnologies could quite feasibly permit the production of such a system with continuous tuning of its relevant structural and magnetic parameters. The purpose is hence to give a detailed understanding of the relation between coherent magnon conductance via the extended well boundary, and the inhomogeneous character, structural and magnetic, of the latter.

The classical magnetic dipolar interactions have not been, in general, an important component in stabilizing bulk magnets, since the strong quantum-mechanical exchange couplings dominate. It is possible that the dipolar interactions may dominate in real nanosystems and for weak exchange. In our model, however, dipole interactions are neglected assuming sufficiently strong exchange.

The present model does not consider thermal effects [20], or effects related to lead connections [25], or inelastic scattering effects due to additional internal degrees of freedom of the nanostructure [26].

The paper is organised as follows. In Section 2 we present the basic elements of the model, describing the spin dynamics in the magnetic films which constitute effectively quasi-2D wave guides, on either side of the atomic well boundary. In Section 3 we study the spin dynamics of the well boundary itself. The transmission and reflection coefficients are then derived, using the matching method [27–29]. In Section 4 numerical applications are presented for three different cases of the local magnetic exchange on the boundary, where we analyse for each case the coherent magnon conductance. The numerical application of the model, and the conclusions that follow, are presented in this section.

2 The model elements

Consider an extended atomic well as shown in Figure 1. The model consists of two magnetic films, each made up of a lattice of three atomic planes, joined by the well. The surface is in the xy-plane, and the y-axis represents a high symmetry direction for the system.

The magnetically ordered system is described by a Heisenberg Hamiltonian, and the spins are taken in the ground state normal to the atomic planes. For ferromagnetic exchange interactions between nearest neighbours, the Hamiltonian may be written as

$$H = -2\Sigma_{p\neq p'} J_{pp'} \boldsymbol{S}_p \cdot \boldsymbol{S}' \qquad (1)$$

$\boldsymbol{S}_p$ ($\boldsymbol{S}_{p'}$) are spin vectors, $|\boldsymbol{S}_p| = S$ for all $p \equiv n, m, s$, which denote integers counting sites along the x, y and z directions. In this notation the sites in Figure 1 read as

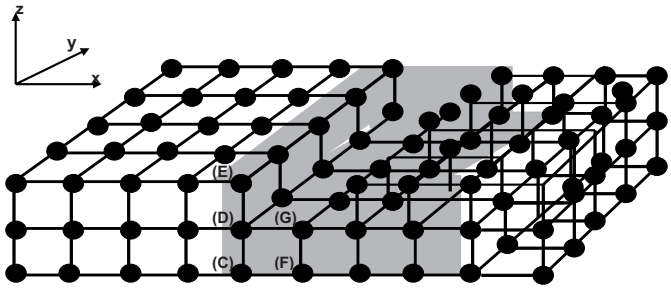

Fig. 1. Schematic representation of an extended atomic well boundary, consisting of two ferromagnetic thin films on either side of the well.

$F(0, 0, 0)$, $G(0, 0, 1)$, $C(-1, 0, 0)$, $D(-1, 0, 1)$, $E(-1, 0, 2)$. Let $J_{pp'} = J$ denote the magnetic exchange between nearest neighbours for all sites in the thin magnetic films. The system is supported on a non-magnetic substrate, and considered otherwise free from magnetic interactions.

The well boundary, delimited over $n \in [-2, +2]$, is an inhomogeneous nanostructure embedded in the thin film. The well boundary may also be considered in general as magnetically inhomogeneous since the local exchange may differ from the rest of the system. This local exchange may be prepared by the insertion of a different type of magnetic ion than that for the rest of the system, also $J_{pp'}$ may be modified by local elastic constraints or by external probes. If J_d denotes the exchange in the well boundary, over $n \in [-2, +2]$, we shall consider three possibilities for $\gamma = J_d/J$, namely $\gamma < 1$ (boundary magnetic softening), $\gamma = 1$, and $\gamma > 1$ (boundary magnetic hardening).

The method used in this paper to study the spin dynamics is based on the equations of motion for the spin precessions for the sites p. Consider the spin precession $\zeta^{\pm}{}_p(t) = \zeta_{px}(t) \pm i\zeta_{py}(t)$, where $\zeta_{p\alpha}(t) = S_{p\alpha}(t) - \langle S_{p\alpha}\rangle$, the brackets denote thermal averages, and α denotes the Cartesian directions. The details of this method are described elsewhere [18].

For sites inside the magnetic films distant from the boundary, over $n \leq -3$ and $n \geq 3$, the equations for spin dynamics, may be cast in the form

$$[\Omega \boldsymbol{I} - D(\exp(i\phi_y), \eta_x)]|\zeta^{\pm}{}_p\rangle = 0. \qquad (2)$$

$\Omega = \omega/\omega_0 = \hbar\omega/2JS$ is a dimensionless frequency for the magnetic films. $\boldsymbol{I}$ denotes a unit matrix, and $D(\exp(i\phi_y), \eta_x)$ is a spin dynamics matrix for the magnetic film lattice. The normalised wave vector $\phi_y = k_y a$, where a is the lattice parameter, runs over the first Brillouin zone in the domain $[-\pi, \pi]$, and η is a generic phase factor between neighbouring sites along the x-direction. In this representation $|\zeta^{\pm}{}_p\rangle$ is the vector of the spin precessions for a unit cell in the magnetic films.

The eigenmodes of equation (2) are characterized by $\exp(\pm i\phi_y)$ phase factorsalong the y-axis, and by the phase factor doublets $\{\eta_x, \eta_x^{-1}\}$ along the x-axis. The propagating magnons correspond to $|\eta_x| = 1$, in which case we can write $\eta_x = \exp(i\phi_x)$, where $\phi_x = k_x a$ runs over the $BZ[-\pi, \pi]$. In contrast, the evanescent eigenmodes are determined from the condition $|\eta_x| < 1$ [29].

These eigenmodes are calculated in general as a function of the frequencies Ω and the normalized wave vectors ϕ_y, when the secular equation of the spin dynamics matrix $[\Omega \boldsymbol{I} - D(\exp(i\phi_y), \eta_x)]$ vanishes. For the system under study the secular equation may be expressed as a polynomial in η_x

$$\Sigma A_s(\exp(i\phi_y), \Omega)\eta_x^s = 0. \quad (3)$$

$A_s(\exp(i\phi_y), \Omega)$ are the polynomial coefficients, $s = 1, 2, 3$. Due to the Hermitian nature of the spin dynamics in the absence of strong external magnetic fields, both η_x and η_x^{-1} verify symmetrically the polynomial forms in the magnetic films.

The solutions of equation (3) yield the eigenmodes $\{\eta_{xj}\}$ of the system, $j \in \{1, 2, 3\}$. For the non propagating eigenmodes, only the evanescent modes $|\eta_{xj}| < 1$ are retained, the divergent ones considered non-physical. There are, hence, only three modes of physical interest. The magnetic films may be seen as effectively wave guides that confine the magnons along the z-direction.

3 Boundary spin dynamics and scattering

To analyse the scattering in the presence of an embedded nanostructure, such as the extended well in Figure 1, it is essential to know the evanescent $|\eta_{xj}| < 1$, as well as the propagating solutions $|\eta_{xj}| = 1$, for a complete description of the scattering processes. In the absence of strong interactions between the elementary spin excitations in the films, these do not couple and we can treat the scattering problem for each eigenmode separately.

For a magnon η_{xj} incident along the x-direction at a given ϕ_y and frequency Ω, the scattering at the boundary yields coherent reflected and transmitted fields.

Let $r_{jj'}$ and $t_{jj'}$ denote the reflection and transmission coefficients that describe the scattering from incident mode j into mode j'. For sites in the films distant from the boundary, the spin precessions field $\{\zeta_p^{\pm}\}$, $n \leq -3$, and $n \geq 3$, may be expressed in terms of an appropriate superposition of the eigenmodes of the perfect film at the same frequency.

Consider a Hilbert space constructed from the basis vectors $[|\boldsymbol{R}\rangle, |\boldsymbol{T}\rangle]$ for reflection and transmission into different eigenmodes, and let $|\zeta^{\pm}{}_p(\text{nanowell})\rangle$ group the spin precessions for an irreducible set of sites in the boundary, $n \in [-2, +2]$. The equations of motion for the boundary domain, coupled to the rest of the system, may hence be written in terms of the composed vector $[|\zeta^{\pm}{}_p(\text{nanowell})\rangle, |\boldsymbol{R}\rangle, |\boldsymbol{T}\rangle]$.

Using the matching approach [29], and the appropriate transformations that relate the spin precessions field in the matching and then film domains, then yields a square inhomogeneous matrix form

$$[\Omega \boldsymbol{I} - D(\exp(i\phi_y), \{\eta_{xj'}\}, \gamma)][|\zeta^{\pm}{}_p(\text{nanowell})\rangle, |\boldsymbol{R}\rangle, |\boldsymbol{T}\rangle] = -|\boldsymbol{IH}, \eta_{xj}\rangle. \quad (4)$$

The vector $-|\boldsymbol{IH}, \eta_{xj}\rangle$, mapped appropriately onto the basis vectors in the constructed Hilbert space, regroups the inhomogeneous terms describing the incident magnons. As pointed out earlier, γ describes the hardening or softening of the local exchange on the well boundary.

The reflection and transmission processes under study are described in terms of the scattering matrix elements [12,13], and these are given explicitly for any given incident magnon j, by the reflection coefficients $\{R_{jj'}\} \equiv |\boldsymbol{R}\rangle$ for the reflected magnons j', and the transmission coefficients $\{T_{jj''}\} \equiv |\boldsymbol{T}\rangle$ for the transmitted magnons j'. The solutions of equation (4) give the reflection, $R_{jj'}$, and transmission coefficients, $T_{jj'}$, in the magnetic films. They also give the spin precessions vector $[|\zeta^{\pm}{}_p(\text{nanowell})\rangle$ for the irreducible set of spins of the boundary.

To compare theory and measurement, we need to calculate the reflection and transmission cross sections $r_{jj'}$ and $t_{jj'}$, and these are calculated at the scattering frequency Ω, in the form

$$\begin{aligned} r_{jj'} &= (v_{gj'}/v_{gj})|R_{jj'}|^2 \\ t_{jj'} &= (v_{gj'}/v_{gj})|T_{jj'}|^2. \end{aligned} \quad (5)$$

The scattering cross sections are normalised with respect to the group velocities of the magnons to obtain unitarity for the scattering matrix. v_{gj} is the group velocity of the eigenmode j, it is equal to zero for evanescent modes.

Furthermore, it is possible to define total reflection and transmission cross sections for a given eigenmode j at frequency Ω, by summing over all the contributions of the scattered magnons

$$\begin{aligned} r_j(\phi_y, \Omega) &= \Sigma_{j'} r_{jj'}(\phi_y, \Omega) \\ t_j(\phi_y, \Omega) &= \Sigma_{j'} t_{jj'}(\phi_y, \Omega). \end{aligned} \quad (6)$$

In order to describe the overall transmission of a mesoscopic multichannel system at a given frequency Ω, it is also useful to define the total magnon boundary conductance, or transmittance, $\sigma(\phi_y, \Omega)$

$$\sigma(\phi_y, \Omega) = \Sigma_j \Sigma_{j'} t_{jj'}(\phi_y, \Omega). \quad (7)$$

The sum is carried out over all input and output channels at the frequency Ω and angle ϕ_y. The transmission scattering cross section $t_j(\phi_y, \Omega)$ per incident magnon j, and the conductance of the system $\sigma(\phi_y, \Omega)$, are important quantities to calculate as each corresponds to an experimentally measurable observable.

4 Numerical applications and discussion

The film magnons may be calculated for any given choice of the normalized wave vector ϕ_y, and their dispersion branches presented as a function of ϕ_y. There are in general three magnon branches in the present case, and these may be symmetric or asymmetric with respect to the central axis along the x-direction. Symmetric modes correspond to spin precessions that satisfy the conditions $\zeta^{\pm}{}_{n,m,N} = \zeta^{\mp}{}_{n,m,N\pm1}$, whereas asymmetric modes satisfy the condition $\zeta^{\pm}{}_{n,m,N} = \zeta^{\pm}{}_{n,m,N\pm1}$, and N is the total number of atomic planes along the z-axis.

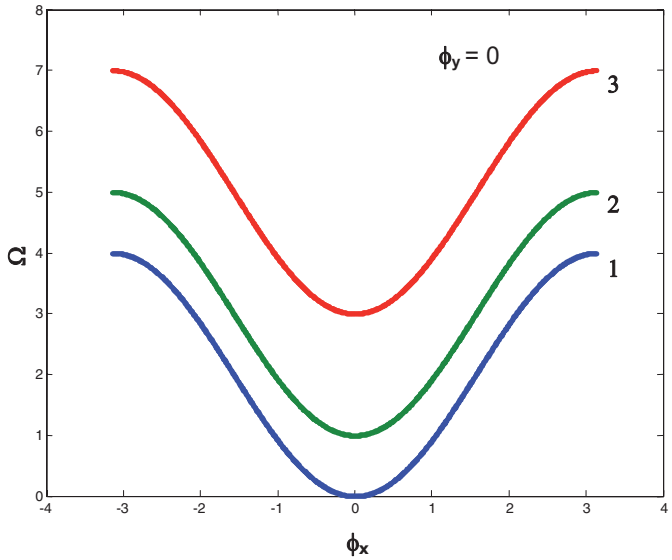

Fig. 2. Magnon dispersion curves for the ferromagnetic thin films made up of three magnetically ordered layers, presented for the special case of $\phi_y = 0$ as a function of ϕ_x in its BZ.

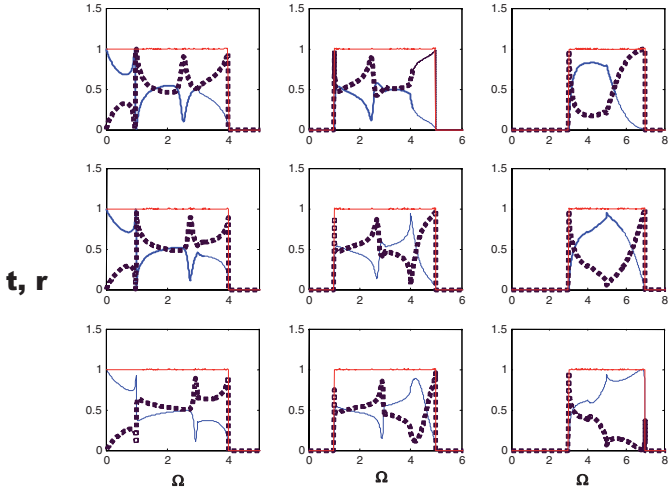

Fig. 3. Numerical results for the reflection and transmission scattering cross sections, for magnon modes $j = 1$, 2 and 3, for $\phi_y = 0$, as a function of the dimensionless frequency Ω. See text for details.

4.1 $\phi_y = 0$

Typical magnon dispersion branches, $j = 1$, 2, 3, are presented in Figure 2 for $\phi_y = 0$. These are propagating modes in the frequency intervals

$$\Omega_1 = [0, \Omega_{1,max} = 4]$$
$$\Omega_2 = [1, \Omega_{2,max} = 5]$$
$$\Omega_3 = [3, \Omega_{3,max} = 7].$$

There is one acoustic mode, $j = 1$, which frequency tends to zero when ϕ_y tends to zero, and two optical modes, $j = 2$, 3.

The numerical results for the scattering effects are presented for three different possibilities as regards the local magnetic exchange, $\gamma = J_d/J$, on the well boundary, namely for $\gamma = 0.9$ (magnetic softening on the boundary), $\gamma = 1$ (homogeneous magnetic exchange throughout the system), and $\gamma = 1.1$ (magnetic hardening on the boundary).

The numerical results for the reflection and transmission scattering cross sections are presented in Figure 3 for the respectively incident magnons modes $j = 1$, 2, and 3. The individual figures are arranged in rows for the variation of the local magnetic exchange, from softening at the top row to hardening at the bottom, and in columns per magnon mode, ranging from 1 at the left to 3 at the right. The transmission (continuous) and the reflection (dotted) cross sections verify the unitarity condition for the scattering matrix, and this is used throughout as a check on the numerical calculation. For each case, we present, for comparison, the transmission histogram per magnon mode for the magnetic films. It is important to distinguish between the spectral features which appear at $\Omega = 0$, 1, 3, 4, 5, 7, and which correspond to the effects coming from the boundaries of the propagating interval for the magnons, at the chosen wave vector ϕ_y, from other spectral features.

From a study of the spectra for modes 1 and 2, we note that the maxima and minima of their reflection and transmission spectra are displaced to higher frequencies in the domain $\Omega =\sim [2.5, 2.9]$, with increasing local magnetic exchange on the boundary. This is the signature for a Fano resonance, and attests to the occurrence of a localized spin mode on the well boundary. It is interesting to note that the two modes 1 and 2 interact with this localized mode, whereas the third mode 3 shows no such resonance in its spectra, since its minimum frequency in its propagating interval lies beyond the domain. The behaviour of the acoustic mode in the left column is otherwise different from that of the optic modes in the two columns to the right. Whereas the transmission cross section decreases for mode 1 with increasing γ, it increases significantly for modes 2 and 3. This shows how reinforcing the magnetic exchange on the well boundary can offset the scattering effects due to the defect boundary, at least for the optic magnons.

4.2 $\phi_y = \pi/4$

Numerical results are presented next for the choice of $\phi_y = \pi/4$. In this case the propagating magnons appear in the frequency intervals

$$\Omega_1 = [0.55, \Omega_{1,max} = 4.55]$$
$$\Omega_2 = [1.55, \Omega_{2,max} = 5.55]$$
$$\Omega_3 = [3.55, \Omega_{3,max} = 7.55].$$

The numerical results for the reflection and transmission scattering cross sections are presented in Figures 3a – 3c for incident magnons $j = 1$, 2, and 3, respectively, and for the three possibilities of the local magnetic exchange on the boundary, namely $\gamma = 0.9$, $\gamma = 1$, and $\gamma = 1.1$. It is useful to note that frequencies $\Omega = 0.55$, 1.55, 3.55, 4.55,

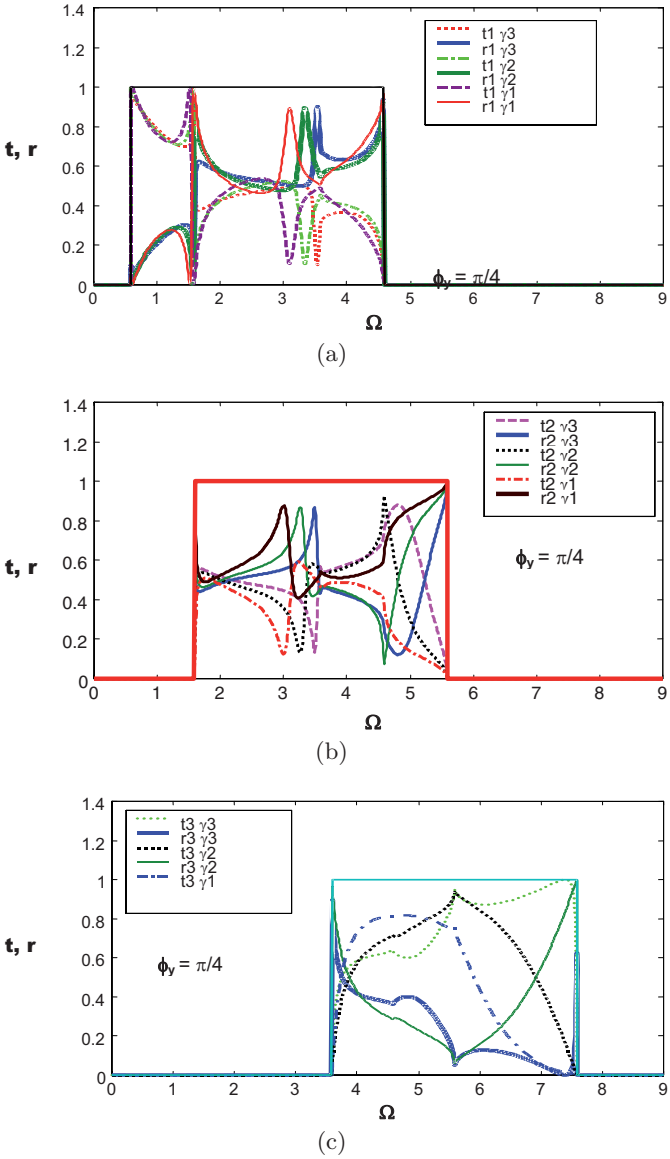

Fig. 4. (a) The calculated reflection r_1 and transmission t_1 cross sections for the acoustic magnon mode incident on the extended well at $\phi_y = \pi/4$, for the three possibilities of local magnetic exchange on the boundary, $\gamma = 0.9$, 1, and 1.1. (b) As in (a), presenting here the calculated reflection r_2 and transmission t_2 cross sections for the optic magnon $j = 2$, incident on the extended well. (c) As in (a), presenting here the calculated reflection r_3 and transmission t_3 cross sections for the optic magnon $j = 2$, incident on the extended well.

5.55, 7.55, correspond to the boundaries of the propagating intervals for these magnons, for $\phi_y = \pi/4$.

Figure 4a presents the reflection and transmission cross sections for magnon $j = 1$. This is the acoustic mode propagating in the interval $\Omega_1 = [0.55, \Omega_{1,max} = 4.55]$, along the x-direction. Up to $\Omega \approx 1.55$ the reflection (transmission) cross sections $r_1(t_1)$, are quite comparable for all three values of the local magnetic exchange on the boundary. This is probably due to the total absence of other propagating magnons in its frequency interval, also to the properties of the acoustic magnon at relatively long wavelengths. The critical changes in the spectra that show up for $\Omega \approx 1.55$ do not correspond to a Fano resonance since they are unaffected by the variation of the local magnetic exchange on the boundary. The minima (in transmission) and maxima (in reflection) are essentially due to the interaction on the boundary between the acoustic mode and the optic mode $j = 2$ which sets in as a propagating mode at $\Omega = 1.55$ for the interval $\Omega_2 = [1.55, \Omega_{2,max} = 5.55]$. The behaviour of the reflection r_1, and transmission t_1, cross sections for the mode $j = 1$, changes strongly for frequencies $\Omega > 1.55$, as the cross sections undergo considerable variation with the changes of the local magnetic exchange on the boundary. Furthermore, the minima of the transmission spectra are displaced to higher frequencies in the domain $\Omega =\sim [3, 3.5]$ with increasing γ. This is the signature for a Fano resonance, and attests again to the occurrence of a localized spin state on the boundary.

Similarly, Figure 4b presents the reflection and transmission cross sections for the magnon $j = 2$, for the three considered γ possibilities. This is an optic mode propagating along the x-direction in its interval $\Omega_1 = [1.55, \Omega_{1,max} = 5.55]$. The minima of the transmission cross section, t_1, present a Fano like resonance and are displaced to higher frequencies with increasing γ, in the frequency domain $\Omega =\sim [3, 3.5]$. This confirms the existence of a localized spin mode on the atomic well boundary. For $\Omega > 3.5$, the transmission and reflected spectra of the optic magnon $j = 2$, present a complicated behaviour. $\Omega = 3.55$ marks the frequency at which the second optic magnon $j = 3$, comes in as a propagating mode. This explains the sudden modifications in the spectra around this frequency due to the interaction at the boundary between the two optic magnons. However, there is an additional complexity arising from γ effects. And we distinguish for $\Omega > 3.55$, two types of behaviour. For magnetic softening, the reflection cross section r_1 increases relatively monotonically with increasing frequency for $\Omega \geq 3.55$ and the transmission cross section t_1 decreases correspondingly. In contrast for magnetic hardening, and even for $\gamma = 1$ which represents a homogeneous magnetic exchange throughout the system, the reflection cross sections r_1 decrease up to $\Omega \sim 4.7$, then increase to unity at the upper limit $\Omega_{2,max} = 5.55$ of the propagating interval for this magnon. Nevertheless, the rapidly changing and the varying behaviour of r_2 and t_2 with the γ variations, does not signal a localized spin mode on the boundary in this frequency domain.

Figure 4c presents the reflection and transmission cross sections for the magnon mode $j = 3$. This is the optic mode propagating along the x-direction in the interval $\Omega_3 = [3.55, \Omega_{3,max} = 7.55]$ for $\phi_y = \pi/4$. Again there is no evidence for Fano resonances and localized spin modes on the boundary domain. The scattered spectra for the reflection r_3 and transmission t_3 cross sections do however suffer important changes across the fixed reference point $\Omega_{2,max} = 5.55$, when the optic magnon $j = 2$ becomes evanescent. Less important changes in this spectra also manifest themselves across the fixed reference

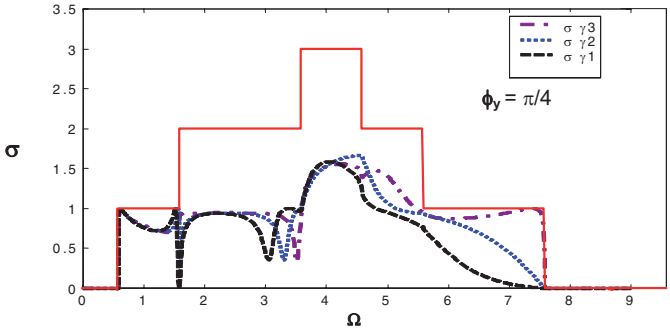

Fig. 5. The calculated total magnon conductance, $\sigma(\phi_y, \Omega)$, across the inhomogeneous well boundary, for magnons incident from within the very thin magnetic films under study. The histogram corresponds to the magnon conductance in the thin magnetic films.

point $\Omega_{1,max} = 4.55$ for magnetic hardening, and even for $\gamma = 1$ which represents a homogeneous magnetic exchange throughout the system.

The total magnon conductance of the system $\sigma(\phi_y, \Omega)$, is useful to calculate, as it corresponds to an experimentally measurable quantity, for example for thermal transport across such embedded nanostructures. $\sigma(\phi_y, \Omega)$ is calculated for the three analysed possibilities of the local magnetic exchange. The numerical results are presented in Figure 5. The conductance is consistently less or equal to two magnons throughout the frequency domain $\Omega \in [0.55, 7.55]$. Another general feature of the total conductance is that it increases with increasing γ, which is to be expected as this corresponds to increasing short range order on the joint nanostructure between the two thin magnetic films. Note that the presence of a Fano resonance and a corresponding localized spin state is further confirmed in the frequency domain $\Omega =\sim [2.8, 3.55]$.

In conclusion, we present a detailed theoretical model for the study of the coherent magnon transport via an atomic well boundary between very thin magnetically ordered films. The spins are taken as ordered normal to the film surface. In particular, we have specifically investigated the influence of the changing inhomogeneous boundary conditions, and of the angle of incidence for film magnons, on the scattering properties across the embedded extended well for these incident magnons. The conductance characteristics of Fano resonances are shown to be specific to the system geometry, and these resonances play a corresponding and characteristic preferential role for the overall magnon conductance spectral features. The evaluation of the thermal transport due to magnon conductance is a straightforward calculation, but is not our primary objective in this paper. It is also possible that the magnon scattering properties could change if the spins are chosen to be ordered along the x-direction rather than the z-direction, and this is the subject of a future publication.

Two of the authors, R.T. and B.B. would like to thank the University of Tizi Ouzou for financial support, and the Université du Maine for their study visit. A.K. should also like to thank the Department of Physics at McGill for his stay.

References

1. V. Shchukin, D. Bimberg, Rev. Mod. Phys. **71**, 1125 (1999)
2. B. Gambardella, M. Blanc, L. Burgi, K. Kuhnke, K. Kern, Surf. Sci. **449**, 93 (2000)
3. K. Kern, H. Niehaus, A. Schatz, P. Zeppenfeld, J. Goerge, G. Comsa, Phys. Rev. Lett. **67**, 855 (1991)
4. S. Rousset et al., Materials Sc. Eng. B **96**, 169 (2002)
5. P. Gambardella, A. Dallmeyer, K. Maiti, M. C. Malagoli, S. Rusponi, P. Ohresser, W. Eberhardt, C. Carbone, K. Kern, Phys. Rev. Lett. **93**, 077203 (2004)
6. A. Vindigni, A. Rettori, M.G. Pini, C. Carbone, P. Gambardella, Appl. Phys. A **82**, 385 (2006)
7. N. Weiss, T. Cren, M. Epple, S. Rusponi, G. Baudot, A. Tejeda, V. Repain, S. Rousset, P. Ohresser, F. Scheurer, P. Bencok, H. Brune, Phs. Rev. Lett. **95**, 157204 (2005)
8. J.N. Crain, D.T. Pierce, Science **7**, 703 (2005)
9. L. Bürgi, O. Jeandupeux, A. Hirstein, H. Brune, K. Kern, Phys. Rev. Lett. **81**, 5370 (1998)
10. Y. Hasegawa, P. Avouris, Phys. Rev. Lett. **71**, 1071 (1993)
11. J. Repp, G. Meyer, K.H. Rieder, Phys. Rev. Lett. **92**, 036803 (2004)
12. R. Landauer, IBM J. Res. Dev. **1**, 223 (1957); R. Landauer, Philos. Mag. **21**, 863 (1970)
13. M. Büttiker, Phys. Rev. Lett. **57**, 1761 (1986)
14. E. Tekman, P.F. Bagwell, Phys. Rev. B **48**, 2553 (1993)
15. C. Berthod, F. Gagel, K. Maschke, Phys. Rev. B **50**, 18 299 (1994)
16. A. Fellay, F. Gagel, K. Maschke, A. Virlouvet, A. Khater, Phys. Rev. B **55**, 1707 (1997)
17. M. Belhadi, A. Khater, O. Rafil, J. Hardy, R. Tigrine, Phys. Stat. Sol. B **228**, 685 (2001)
18. A. Khater, M. Abou Ghantous, Surface Sci. Lett. **498**, L97 (2002); M. Abou Ghantous, A. Khater, Eur. Phys. J. B **12**, 335 (1999)
19. Y. Imry, *Introduction to Mesoscopic Physics* (Oxford University Press, Oxford, 1997)
20. F. Schütz, M. Kollar, P. Kopietz, Phys. Rev. Lett. **91**, 017205 (2003)
21. R.L. Stamps, R.E. Camley, B. Hillerbrands, G. Güntherodt, Phys. Rev. B **46**, 10836 (1992)
22. M. Belhadi, R. Chadli, A. Khater, M. Abou Ghantous, Eur. Phys. J. App. Phys. **37**, 25 (2007)
23. B. Bourahla, A. Khater, R. Tigrine, O. Rafil, M. Abou Ghantous, J. Phys.: Cond. Matter **19**, 266208 (2007)
24. A.R.P. Rau, Physica Scripta **69**, 1 (2004)
25. A. Dhar, B.S. Shastry, Phys. Rev. B **67**, 195405 (2003)
26. Y. Imry, O. Entin-Wohlman, A. Aharony, Europhys. Lett. **72**, 263 (2005)
27. T.E. Feuchtwang, Phys. Rev. **155**, 731 (1967)
28. J. Szeftel, A. Khater, J. Phys. C: Solid State Phys. **20**, 4725 (1987)
29. M. Belhadi, O. Rafil, R. Tigrine, A. Khater, J. Hardy, A. Virlouvet, K. Maschke, Eur. Phys. J. B **15**, 435 (2000)